Impact of Manganese on and Transfer across Blood-Brain and Blood-Cerebrospinal Fluid Barrier *in Vitro**[S]

Julia Bornhorst[‡§], **Christoph A. Wehe**[¶], **Sabine Hüwel**[‖], **Uwe Karst**[¶], **Hans-Joachim Galla**[‖], **and Tanja Schwerdtle**[§1]

From the ‡*Graduate School of Chemistry,* §*Institute of Food Chemistry,* ¶*Institute of Inorganic and Analytical Chemistry,* and ‖*Institute of Biochemistry, the University of Münster, 48149 Münster, Germany*

Background: Modes of neurotoxic action after Mn overexposure are not fully understood.
Results: The blood-CSF barrier showed higher Mn sensitivity and active Mn transport properties.
Conclusion: The blood-CSF barrier might be the major route for Mn into the brain.
Significance: Deeper insight in the impact of Mn on and its transfer across brain barrier systems might help to prevent irreversible neurological damage.

Manganese occupational and dietary overexposure has been shown to result in specific clinical central nervous system syndromes, which are similar to those observed in Parkinson disease. To date, modes of neurotoxic action of Mn are still to be elucidated but are thought to be strongly related to Mn accumulation in brain and oxidative stress. However, the pathway and the exact process of Mn uptake in the brain are yet not fully understood. Here, two well characterized primary porcine *in vitro* models of the blood-brain and the blood-cerebrospinal fluid (CSF) barrier were applied to assess the transfer of Mn in the brain while monitoring its effect on the barrier properties. Thus, for the first time effects of $MnCl_2$ on the integrity of these two barriers as well as Mn transfer across the respective barriers are compared in one study. The data reveal a stronger Mn sensitivity of the *in vitro* blood-CSF barrier compared with the blood-brain barrier. Very interestingly, the negative effects of Mn on the structural and functional properties of the highly Mn-sensitive blood-CSF barrier were partly reversible after incubation with calcium. In summary, both the observed stronger Mn sensitivity of the *in vitro* blood-CSF barrier and the observed site-directed, most probably active, Mn transport toward the brain facing compartment, reveal that, in contrast to the general assumption in literature, after oral Mn intake the blood-CSF barrier might be the major route for Mn into the brain.

Manganese (Mn) is an essential trace element required for normal growth development and cellular homeostasis (1). In the brain, Mn is of central importance as co-factor for a wide variety of enzymes, including arginase, pyruvate carboxylase, the antioxidant enzyme superoxide dismutase, as well as enzymes involved in neurotransmitter synthesis and metabolism. Very interestingly, an imbalance in Mn homeostasis caused by either Mn deficiency or overload is well known to

result in severe CNS dysfunction. However, whereas Mn deficiency is extremely rare in humans, toxicity is more prevalent. Excessive brain Mn promotes potent neurotoxic effects with symptoms including tiredness, behavioral changes, and delayed neurological disturbances characterized by dystonia or kinesia, resembling many clinical features of parkinsonism but also distinct dissimilarities (2); the neurological phenotype is known as manganism (3). A primary source for Mn intoxication is the occupational exposure in miners, welders, or workers in dry-cell battery factories. In addition, individuals receiving total parenteral nutrition, the contrast agent MnDPDP (also called manganese(II) *N*,*N*'-dipyridoxylethylenediamine-*N*,*N*'-diacetate-5,5'-bis(phosphate); mangafodipirtri-sodium; TESLASCAN™), or drinking water with high levels of Mn are at higher risk for Mn intoxication; subtle preclinical neurological effects such as changes in cognitive abilities, short term memory, and motor control have been documented (4–7).

To date, the underlying mechanisms of Mn-induced neurotoxicity are still to be elucidated. Several modes of action are discussed, among others oxidative stress, subsequent DNA damage, and mitochondrial dysfunction in specific brain regions. Manganism is associated with elevated Mn levels in certain brain areas, namely cautate-putamen, globus pallidus, substantia nigra, and subthalamic nucleus (8, 9).

Brain manganese homeostasis is largely regulated by the blood-brain barrier (BBB)[2] and blood-cerebrospinal fluid (CSF) barrier. The BBB separates blood from brain interstitial fluid and consists basically of capillary endothelial cells connected by narrow tight junctions which prevent paracellular flux processes. Moreover, recently it has become evident that the cells of the neurovascular unit, namely astrocytes, pericytes, and neuronal cells are further essential for the induction and maintenance of the BBB properties (10). The second regulating system, the blood-CSF barrier, is built up by the epithelial cells of

[2] The abbreviations used are: BBB, blood-brain barrier; CSF, cerebrospinal fluid; CP, choroid plexus; DIV, day *in vitro*; DMT1, divalent metal transporter 1; FIA-ICP-QMS, flow injection inductively coupled plasma mass spectrometry with quadrupole mass analyzer; PBCEC, porcine brain capillary endothelial cell; PCPEC, porcine choroid plexus cell; SFM, serum-free medium; TEER$_N$, transendothelial electrical resistance; TEER$_P$, transepithelial electrical resistance; TfR, transferrin receptor.

the choroid plexus (CP) and separates blood from the CSF. This epithelial barrier, which is sealed with tight junctions between the epithelial cells at the CSF-facing surface (apical surface) becomes indispensable because the endothelium of the CP is leaky and highly permeable. Despite the CSF secretion, as the best recognized feature of the CP, further CP functions include general brain homeostasis as well as defense of the brain against harmful substances (11).

Although Mn can cross the BBB and the blood-CSF barrier through several carriers in different oxidation states, the exact identity of the transporter(s) responsible as well as the process itself are still strongly debated. How Mn crosses the BBB has been a subject of many studies, and it appears that several pathways are operative, including facilitated diffusion (12) and active transport. Mn is discussed to be transported among others via the divalent metal transporter 1 (DMT1), the transferrin receptor (TfR), the divalent metal/bicarbonate ion symporters ZIP8 and ZIP14, various calcium channels, the solute carrier-39 (SLC39) family of zinc transporters, park9/ATP13A2, the magnesium transporter hip14, the transient receptor potential melastatin 7 (TRPM7) channels/transporters, homomeric purinreceptors (P2X and P2Y), and the citrate transporter (3, 13–16).

In contrast, transfer of Mn across the blood-CSF barrier has been less studied. Proposed transporters include TfR, DMT1, metal transporter protein-1 (MTP1), Ca channels or zinc-transporter (ZnT1, ZnT3, ZnT4, and ZnT6) (summarized in Ref. 16).

Regarding the question of which Mn species enter the brain, Mn(II), Mn(II/III)citrate, and Mn(III)transferrin are likely to be most relevant. Thereby, interestingly the Mn valence status might account for the transport properties at the respective barrier. Whereas Mn(III) enters the brain via TfR-mediated mechanisms, Mn(II) is most likely readily taken up as free ion species or as a nonspecific protein-bound species (17, 18).

In this work, two well characterized cell culture models of the BBB and the blood-CSF barrier were used to assess the transfer of Mn in the brain while monitoring its effect on the barrier properties. These two porcine-based *in vitro* models allow for the first time a direct comparison of the effects of Mn on and the respective Mn transfer across the BBB and the blood-CSF barrier. Thereby, also the different impacts on the barriers are illustrated when $MnCl_2$ is exposed from blood- or brain-facing sides. Furthermore, this paper indicates that the negative effects of Mn on the barrier properties of the highly Mn-sensitive blood-CSF barrier are partly reversible after treatment with Ca-enriched serum-free medium.

EXPERIMENTAL PROCEDURES

Preparation of $MnCl_2$ and $CaCl_2$ Stock Solution—$MnCl_2$ (>99.995% purity) and $CaCl_2$ (> 99% purity) (Sigma-Aldrich) stock solution were prepared in sterile bidistilled water. To prevent oxidation, stock solutions were prepared shortly before each experiment.

Isolation of Primary Porcine Brain Capillary Endothelial and Choroid Plexus Epithelial Cells—Primary porcine brain capillary endothelial cells (PBCECs) were isolated, cultivated and cryopreserved as previously described (19). Primary porcine

choroid plexus cells (PCPECs) were prepared as described before (20) with slight modifications. Briefly, CP tissue from freshly slaughtered pigs was incubated with 0.2% trypsin at 4 °C for 45 min and warmed to 37 °C for 30 min. The release of the epithelial cells from the basal lamina was stopped by adding newborn bovine serum (Biochrom, Berlin, Germany). The cells were centrifuged at $20 \times g$ and resuspended in Dulbecco's modified Eagle's medium (DMEM)/Ham's F-12 (1:1) supplemented with 10% fetal bovine serum (FBS), 4 mM L-glutamine, 100 units/ml penicillin, 100 μg/ml streptomycin (all Biochrom), 5 μg/ml insulin, and 20 mM cytosine arabinoside (both Sigma-Aldrich). The nucleoside analog cytosine arabinoside suppressed the growth of fibroblastic cells (21).

BBB Cell Culture Model—PBCECs were gently thawed and seeded (250,000/cm^2) on rat tail (22) collagen-coated (0.54 mg/ml) Transwell® filter inserts with microporous polycarbonate membranes (Corning, Wiesbaden, Germany, 1.12-cm^2 growth area, 0.4-μm pore size) on day *in vitro* (DIV) 2 in plating medium (Medium 199 Earle supplemented with 10% newborn calf serum (NCS), 0.7 mM L-glutamine, 100 μg/ml gentamycin, 100 units/ml penicillin, 100 μg/ml streptomycin (all Biochrom)) in the apical compartment at 37 °C with 5% CO_2 and 100% humidity. After PBCECs reached confluence (DIV4), the plating medium was replaced by serum-free culture medium (SFM-PBCEC) (DMEM/Ham's F-12 (1:1) containing 4.1 mM L-glutamine, 100 μg/ml gentamycin, 100 units/ml penicillin, 100 μg/ml streptomycin (all Biochrom)) and 550 nM hydrocortisone (Sigma-Aldrich) to induce differentiation. Permeability ([^{14}C]sucrose, $MnCl_2$) and barrier integrity studies were started on day DIV6.

BBB Co-culture Model—A co-culture model of PBCECs and CCF-STTG1 was used as described previously (23). CCF-STTG1 (CCL-1718^{TM}, American Type Culture Collection) cells were cultured in RPMI 1640 medium (Biochrom) containing 10% FBS (PAA Laboratories, Pasching, Austria), 1.4 mM L-glutamine (Biochrom), 100 units of penicillin/ml and 100 μg of streptomycin/ml (PAA Laboratories) at 37 °C with 5% CO_2 and 100% humidity. For the co-culture system, CCF-STTG1 cells were trypsinized and seeded (100,000 cells/cm^2) on the lower side of the microporous Transwell® filter insert (1.12-cm^2 growth area, 3-μm pore size) to simulate a direct co-culture. Six hours later, the inserts were turned around and placed into the well, and PBCECs were seeded on the upper side of the insert, which was coated with rat tail collagen, and the co-culture system was subsequently cultured as described above.

Blood-CSF Barrier Cell Culture Model—PCPECs were seeded on Matrigel^{TM}-coated (Sigma-Aldrich) microporous Transwell® filter inserts in the apical compartment using a seeding density of 30 cm^2/g wet weight of CP tissue (DIV1). Thereafter, medium was changed every second day. On day DIV8, cells reached confluence, and the medium was replaced by serum-free medium (SFM-PCPEC) (DMEM/Ham's F 12 (1:1) supplemented with 4 mM L-glutamine, 100 units/ml penicillin, 100 μg/ml streptomycin, and 5 μg/ml insulin) to allow full cell differentiation. The cells were further supplemented with SFM on DIV11, and barrier integrity and transport studies were started on day DIV13, when the cells were fully differentiated and built up their respective functions (21, 24). PCPECs

started to actively pump medium from the basolateral into the apical chamber, a process that is comparable with the secretion of cerebrospinal fluid *in vivo*, and transported phenol red to the basolateral chamber. Additionally, the transepithelial electrical resistance (TEER$_P$) increased.

TEER and Capacitance Measurements—The transendothelial electrical resistance (TEER$_N$) and the TEER$_P$ were used as parameters for integrity of the respective barriers, measured by the cellZscope® (nanoAnalytics, Münster, Germany) device. The module used was suitable for 24 Transwell® filter system, grown with PBCEC or PCPEC monolayer. The determined capacitance is directly proportional to the plasma membrane surface area. Changes in the basolateral area and changes in protein content and distribution may also contribute to capacitance changes. Only wells with TEER$_N$ values >600 ohms × cm^2 and capacitance values between 0.45 and 0.6 microfarad/cm^2 on day DIV6 indicate a confluent PBCEC monolayer with good barrier properties and were used for the respective experiments. On day DIV13, wells with PCPEC monolayer in which the TEER$_P$ values dropped below 600 ohms*cm^2 and/or capacitance values dropped below 3.3 microfarads/cm^2 were excluded from the respective experiment.

[^{14}C]Sucrose Permeability—Another technique to analyze barrier integrity is the determination of the permeability for radiolabeled [^{14}C]sucrose through the endothelial or epithelial cell layer. Because sucrose is not taken up by endothelial and epithelial cells either by active or facilitated transport, the permeability for sucrose solely depends on the paracellular barrier tightness. At defined time points, as indicated in the respective experiments, radiolabeled [^{14}C]sucrose (Amersham Biosciences) was added to the apical side of the Transwell® filter. By measuring the time-dependent amount of [^{14}C]sucrose that passes to the basolateral side, the permeability was calculated as described previously (22).

Manganese-induced Effects on and Transfer over Barrier Models—To study the impact of Mn on the barrier integrity as well as Mn transfer across the accomplished *in vitro* barriers, the respective *in vitro* models were exposed to MnCl$_2$ either on the apical or on the basolateral side or on both sides simultaneously. MnCl$_2$ was applied by replacing 10% of the apical and/or basolateral medium by a freshly prepared MnCl$_2$ solution to finally reach concentrations of 1–500 μM MnCl$_2$ as described in the respective experiments. During the following 72 h of incubation, aliquots were sampled from the apical and basolateral compartments for the flow injection inductively coupled plasma mass spectrometry with quadrupole mass analyzer (FIA-ICP-QMS) measurements while monitoring online the respective TEER$_{N/P}$ and capacitance values. Finally, Mn transfer from one compartment to the other was expressed in percentage (in relation to the applied concentration), as concentration (in micromolar) in each of the compartments as well as in case a time-dependent linear correlation as permeability coefficients in centimeters/second (25). Regarding blood-CSF barrier, function of the barrier was additionally assessed by determination of the absorbance (558 nm, NanDrop 1000, PEQLAB Biotechnologie GMBH, Erlangen, Germany) of phenol red in the respective compartments.

In a further, preliminary experiment the DMT1 inhibitor NSC306711 was used to assess the role of DMT1 in the Mn transfer across the blood-CSF barrier. Therefore, the inhibitor stock solutions were prepared in dimethyl sulfoxide, and the basolateral compartments of the blood-CSF *in vitro* barrier model were incubated with 5, 10, 50, and 100 μM NSC306711 (with a final dimethyl sulfoxide concentration ≤1%) immediately prior to the basolateral incubation with MnCl$_2$ (10, 25 μM). Additionally, basolateral incubation with 1% dimethyl sulfoxide was carried out as vehicle control.

The role of the Na$^+$,K$^+$-ATPase in Mn transfer was examined incubating 200 nM selective Na$^+$,K$^+$-ATPase inhibitor ouabain in the basolateral compartment of the blood-CSF *in vitro* barrier model immediately prior to the basolateral or apical incubation with 10 μM MnCl$_2$.

To study the impact of Ca-enriched media on Mn-induced disturbance of blood-CSF barrier properties, Transwell® filters with PCPEC monolayers were preincubated with 200 μM MnCl$_2$ at the basolateral compartment for 24 h. Thereafter, the respective basolateral media were kept for further 72 h or replaced by either fresh SFM or by fresh SFM enriched with 250 or 500 μM CaCl$_2$ and postincubated for 72 h.

Immunocytochemistry—Immunocytochemistry studies were performed with PCPEC monolayers grown on the Transwell® filters as described previously (26, 27). 1 μg/ml mouse anti-occludin (Zytomed, Berlin, Germany) and 5 μg/ml mouse anti-Na$^+$,K$^+$-ATPase (Upstate Biotech) were applied at 37 °C in a 0.5% BSA (Roth, Karlsruhe, Germany) solution for 30 and 90 min, respectively.

The secondary antibody Alexa Fluor 546 goat anti-mouse (1 μg/ml) (Invitrogen) was also diluted in 0.5% BSA and incubated for 1 h at 37 °C. Additionally, cell nuclei were stained with 10 μg/ml Hoechst 33258 (bisbenzimide; Sigma-Aldrich) for 0.5 min. Filters with immunostained cells were cut out from the inserts and mounted in Aqua Poly/Mount (Polysciences). Pictures were taken with the fluorescence microscope Axio ImagerM2 (Zeiss) and evaluated with Axiovision 4.5 software (Zeiss).

Cytotoxicity Testing of MnCl$_2$—Cytotoxic effects of MnCl$_2$ on PBCECs and PCPECs were evaluated using the neutral red uptake assay. This assay is based on the ability of viable cells to incorporate and bind the supravital dye neutral red in the lysosomes (28). PBCECs and PCPECs were cultured in 96-well culture plates, which in case of PBCECs were coated with rat tail collagen. Thereby, all culture conditions including media and cell density were absolutely analogous to the below mentioned cultivation of the respective cells on Transwell® filters as well as to the cellular bioavailability studies. Incubation of PBCECs and PCPECs with MnCl$_2$ was performed on DIV6 and DIV13, respectively. After 24- or 72-h incubation, the medium was replaced by neutral red (3-amino-7-dimethylamino-2-methyl-phenazine hydrochloride) containing medium (70 mg/liter neutral red (Sigma-Aldrich) in SFM used for the respective cells). After dye loading (37 °C, 3 h), cells were washed with phosphate-buffered saline (PBS) containing 0.5% formaldehyde (Roth, Karlsruhe, Germany). The incorporated dye was solubilized in 100 μl of acidified ethanol solution (50% ethanol, 1% acetic acid in PBS), and finally the absorbance in each well was

TABLE 1

ICP-QMS parameters used for FIA measurements

Power	1550 W
Cool gas flow	14 liters/min
Auxiliary gas flow	0.8 L/min
Nebulizer gas flow	≈1 liter/min
Nebulizer type	μFlow PFA-ST (ESI, Omaha, NE)
Injector inner diameter	1.8 mm
Spray chamber type	Cyclone @ 2.7 °C
Mode	CCT[ED]
Cell gas	7% H_2 in He (purity > 99.999%)
Cell gas flow	≈5 ml/min
Δbias	3 V
Dwell time	50 ms @ 1 channel

FIGURE 1. **Cytotoxicity of MnCl$_2$ in confluent PBCECs and PCPECs after 24- or 72-h incubation.** Cytotoxicity was determined by a decrease in the cell viability as determined by the neutral red uptake assay. The data represent mean values of at least three independent determinations with six replicates each ± S.D. (*error bars*).

measured by a plate reader (FLUOstar Optima, BMG Labtechnologies, Jena, Germany) at 540 nm.

Manganese Quantification in Cells and Media—Cellular Mn content was determined after ashing of cells by inductively coupled plasma mass spectrometry (ICP-MS). Due to the low number of cells used and the low Mn concentrations applied in the barrier studies, we were not able to quantify the total Mn content in cells grown on Transwell® filters, but had to use cells, which were grown in culture flasks. Briefly, after 48-h incubation with MnCl$_2$, PBCECs grown on rat tail collagen-coated culture flasks (25 cm^2) or PCPECs grown on culture flasks (25 cm^2) were washed twice with PBS (37 °C) and incubated 15 min on ice with 300 μl of radioimmuneprecipitation assay buffer (0.01 M Tris (pH 7.6), 0.15 M NaCl, 0.001 M EDTA, 0.001 M PMSF, 1% sodium desoxycholate, 1 mg/ml aprotinin, 1 μg/ml leupeptin, 1 μg/ml, pepstatin, 0.1% SDS (all Sigma-Aldrich)). Cells were scraped off and sonicated on ice, and the cell suspension was centrifuged at 15,000 × g (4 °C) for 20 min; in an aliquot of the supernatant, the cellular protein level was quantified by the Bradford assay. Subsequently, the cell suspension was mixed again, evaporated, and incubated with the ashing mixture (65% HNO$_3$/30% H$_2$O$_2$ (1/1) (both Merck)) at 95 °C for at least 12 h. After dilution of the ash with bidistilled water, the Mn concentration was determined by FIA-ICP-QMS. This method has been established previously by our group (29) and was applied in the present work to quantify Mn in cells as well as media sampled from the barrier studies. Briefly, the respective samples were incubated with rhodium (final concentration 10 μg/liter) as internal standard, to compensate drift effects and variations of injected volumes, and further diluted 10-fold with bidistilled water before injection. The FIA approach consisted of a liquid chromatography (LC) system without a column mounted, which was coupled with an ICP-QMS. The LC system combined a quaternary low pressure gradient LC pump (AccelaPump1250™) and a corresponding autosampler (AccelaAutosampler™) whose 6-port stainless steel injection valve was connected to the nebulizer of the ICP-QMS (iCAP Qc™) via a polyether ether ketone capillary (inner diameter, 0.13 mm). All instruments were manufactured by Thermo Scientific. The parameters for the Mn measurements with FIA-ICP-QMS are provided in Table 1. The calculated lowest detection limits for Mn in the respective SFM of the applied barrier models were 2.7 and 6.8 μg/liter, respectively.

RESULTS

Cytotoxicity Testing—In PCPECs, Mn showed no cytotoxicity as measured by the neutral red uptake assay after 24- and
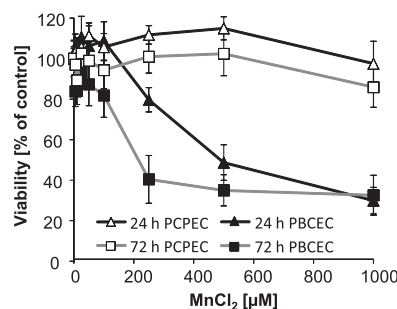
72-h incubation with up to 1000 μM MnCl$_2$ (Fig. 1). In contrast, in PBCECs cellular viability declined in a concentration- and time-dependent manner. The online measurement of the electrical capacitance further confirmed cytotoxicity of MnCl$_2$ in PBCECs by a concentration-dependent increase (data not shown).

Manganese Bioavailability—The applied culture media contained 0.03 μM ± 0.01 μM Mn, which is comparable with the reported normal Mn contents in human serum (30). Total Mn concentrations in nonexposed cells were comparable in both cell types, whereas after 48-h MnCl$_2$ incubation, cellular total Mn concentration was about 3-fold lower in PBCECs compared with PCPECs (Table 2). Thus, very interestingly, even though showing lower cellular Mn bioavailability, PBCECs are more sensitive toward Mn cytotoxicity compared with PCPECs.

MnCl$_2$ and BBB—In the first set of experiments, a well characterized cell culture model of the BBB consisting of PBCECs (19, 22) was incubated with increasing concentrations of MnCl$_2$. The PBCECs were grown on Transwell® filter inserts, thereby building up a two-chamber system, which mimics the *in vivo* CNS situation as closely as possible. The apical compartment refers to the blood side *in vivo*, and the basolateral side refers to the brain side. The impact of MnCl$_2$ on the barrier integrity was quantified monitoring the TEER$_N$ values during the entire 72 h of Mn incubation. Incubating MnCl$_2$ on the apical side, impedance analysis (Fig. 2A) indicated no measurable effect on barrier integrity up to an incubation concentration of 100 μM MnCl$_2$. MnCl$_2$ concentrations of 150 and 175 μM strongly decreased TEER$_N$ values within the first 12 h of incubation, but allowed a reconstitution of the barrier integrity in the following hours. In contrast, 200 μM MnCl$_2$ caused an irreversible decrease of the TEER$_N$, indicating an irreversible disruption of the BBB. To verify the results of the TEER$_N$ studies, barrier integrity was additionally determined by [^{14}C]sucrose permeability studies. In case of an apical 72-h incubation with 200 or 300 μM MnCl$_2$, the permeation of [^{14}C]sucrose was about 8–100-fold increased compared with control cells (Fig. 2E), indicating strong barrier leakage and disruption. In case of an incubation on the basolateral side, the tightness of the PBCEC monolayer was not impaired by up to 500 μM MnCl$_2$ (Fig. 2B); similarly permeability for [^{14}C]sucrose was not affected (Fig. 2E).

TABLE 2

Cellular bioavailability of MnCl$_2$ in PBCECs and PCPECs after 48-h incubation

Data represent mean values of at least two independent determinations each with two replicates ± S.D.

Incubated MnCl$_2$	Cellular Mn in PBCECs	Cellular Mn in PCPECs
μM	*μg Mn/mg protein*	*μg Mn/mg protein*
0	0.20 ± 0.03	0.20 ± 0.01
50	1.14 ± 0.18	3.33 ± 0.05
200	2.90 ± 0.76	7.63 ± 1.76

For better understanding, Mn barrier transfer results are shown in the respective figures expressed in terms of Mn concentrations in the acceptor compartment (Fig. 2C), as percentage permeability in relation to the applied concentration (Fig. 2D) and as permeability coefficient (Fig. 2E). In case of adding ≤100 μM MnCl$_2$ to the apical compartment, after 24–72 h, Mn concentrations increased in a linear-dependent manner in the basolateral compartment (Fig. 2C). Fig. 2D shows the corresponding crossover of approximately 15% within 24 h and approximately 30% within 72 h, which relates to a permeability coefficient of $1.40*10^{-6} \pm 1.07*10^{-7}$ cm/s (Fig. 2E). Due to the leakage of the barrier after incubation with MnCl$_2$ concentrations >100 μM on the apical side (Fig. 2A), a Mn concentration equation between the compartments (Fig. 2D) and thus increased permeability coefficients of up to $3.52*10^{-6} \pm 3.45*10^{-7}$ cm/s (300 μM MnCl$_2$) (Fig. 2E) were achieved.

Because in literature very little is known about Mn movement out of the brain into the blood MnCl$_2$ was added to the basolateral side in a second approach. Our data clearly show that up to MnCl$_2$ concentrations of 50 μM, Mn basolateral-to-apical transfer was indistinguishable from the apical-to-basolateral transfer. This indicates that after incubation on the basolateral or the apical side, Mn crossed the barrier in both directions (apical-to-basolateral and basolateral-to-apical transfer) to a comparable extent. In case of basolateral incubation with concentrations >50 μM MnCl$_2$, respective percentage Mn permeabilities (Fig. 2D) and permeability coefficients (Fig. 2E) were strongly reduced.

In a third approach, MnCl$_2$ was incubated in equal concentrations both to the apical and the basolateral medium. No accumulation was visible in one of the compartments within 72 h of incubation with 50 μM MnCl$_2$, pointing to a passive Mn transfer process (Fig. 2F). The TEER$_N$ analyses showed similar results compared with a MnCl$_2$ incubation on the apical side and thereby also ruled out that the observed effects on the TEER$_N$ values in general were caused by an ionic effect of Mn^{2+}.

In addition to the monoculture BBB experiments, a direct co-culture approach (23) based on the BBB architecture *in vivo* was used, in which brain capillaries are entirely covered by astrocytic feed. After apical MnCl$_2$ incubation, neither the TEER$_N$ analyses nor the transfer experiments showed significant different results compared with the monoculture studies (data not shown).

MnCl$_2$ and Blood-CSF Barrier—The next set of experiments focused on the second cellular interface, which regulates the exchange between the blood and CNS, the blood-CSF barrier. The applied, well established *in vitro* cell culture model of the blood-CSF barrier is built up by PCPECs (20), shows several features of physiological activity, and mimics the *in vivo* situation quite closely (21, 24). In this *in vitro* model, the apical side of the PCPEC layer mimics the ventricular compartment, whereas the basolateral side represents the blood side *in vivo*. For the characterization of the structural and functional properties of the *in vitro* blood-CSF barrier, different parameters were used. The TEER$_P$ and [^{14}C]sucrose permeability were determined to characterize barrier tightness. Functional changes could be shown by the capacitance, the active fluid secretion, and the phenol red concentration in the upper (apical) chamber. Whereas the *in vitro* barrier was not affected after basolateral incubation with up to 25 μM MnCl$_2$, tightness and function of the PCPEC monolayer were concentration-dependently disturbed after basolateral incubation with ≥50 μM MnCl$_2$. Thus, TEER$_P$ and capacitance values decreased (Fig. 3, A and B), pointing to a barrier disruption and a decreased number of PCPECs microvilli, respectively. Moreover, fluid secretion was reduced (data not shown) and phenol red concentration increased on the apical side (Fig. 3C), indicating an adverse effect on the proper function of the organic anion transporter, which is driven by the Na$^+$,K$^+$-ATPase. Barrier leakage was additionally confirmed by the results of the [^{14}C]sucrose permeability studies (Fig. 4C).

Similar to the BBB *in vitro* model, in the blood-CSF barrier model Mn affected barrier integrity stronger after incubation on the blood side. After apical exposure, an impairment of the barrier tightness (Fig. 3D) and function (data not shown) was not visible until 200 μM MnCl$_2$.

The time profiles of the basolateral-to-apical Mn transfer (Fig. 4A) and apical-to-basolateral Mn transfer (Fig. 4B) clearly demonstrate a higher transfer rate from basolateral incubated Mn into the apical compartment compared with the other direction. In case of basolateral incubation with ≤50 μM MnCl$_2$, after 48 h of incubation Mn accumulated in the brain facing compartment, whereas after barrier disruption by 200 μM MnCl$_2$, a concentration equation was achieved between the compartments (Fig. 4A). Because of the missing linear correlation, the basolateral-to-apical Mn transfer could not be expressed as permeability coefficient. Very interestingly, only approximately 20% of the apical dose applied (50, 200 μM MnCl$_2$) reached the basolateral compartment (Fig. 4B) corresponding to permeability coefficients of approximately $1*10^{-6}$ cm/s (Fig. 4C). Further studies, applying an equal MnCl$_2$ concentration (10 μM) in each compartment, demonstrate a Mn accumulation in the apical compartment (Fig. 4D). This clearly points to an active transport mechanism. In the case of a parallel incubation with 200 μM MnCl$_2$, due to a barrier disruption, a concentration equation was achieved between the compartments (Fig. 4D).

To identify possible transport mechanisms for Mn cellular uptake, the well characterized DMT1 inhibitor NSC306711 (31), incubated immediately prior MnCl$_2$ (10, 25 μM) at the basolateral compartment, was used. Considering experiments with fully intact barriers in the presence of ≤50 μM
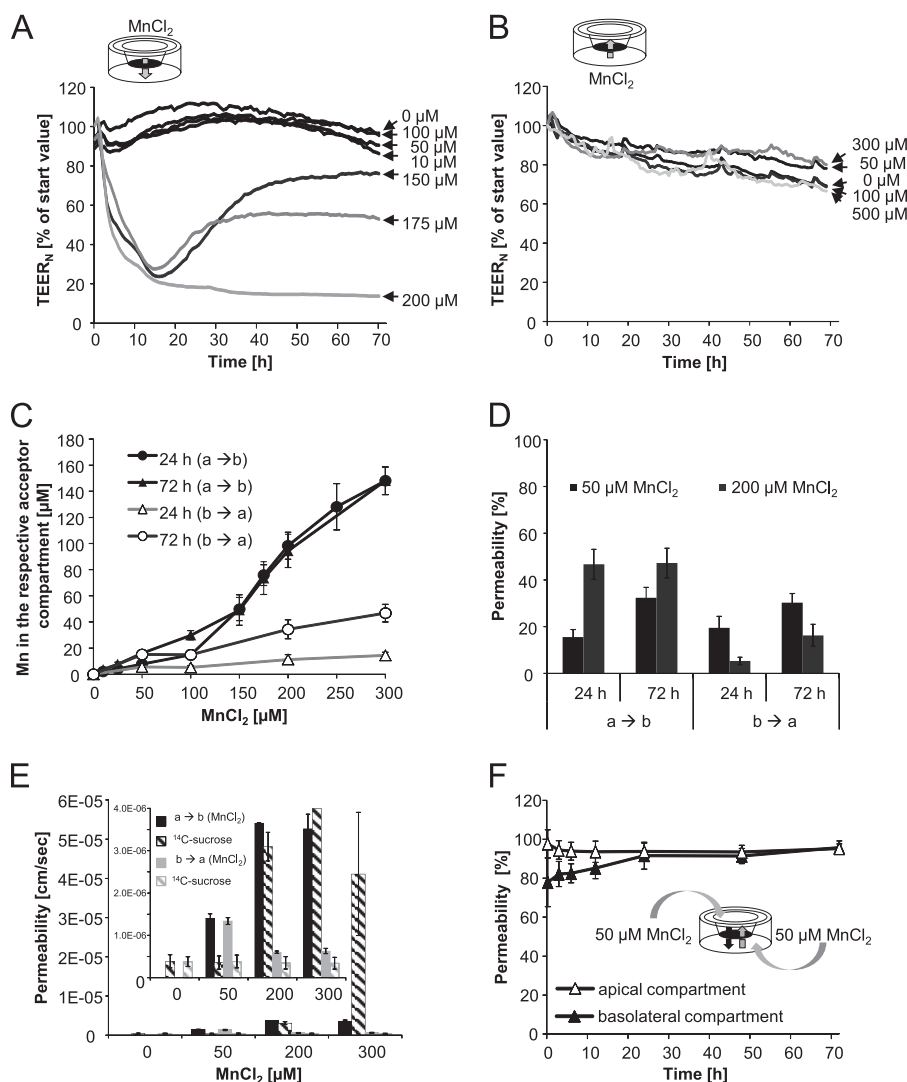
FIGURE 2. **Mn and *in vitro* BBB.** *A* and *B*, impact of MnCl$_2$ on the barrier integrity as measured by TEER$_N$ values after application of MnCl$_2$ either on the apical (influx studies) (*A*) or the basolateral compartment (efflux studies) (*B*). Data, expressed as percentage of start value, represent mean values of at least three independent determinations with three replicates each with S.D. $< \pm10\%$. Mean TEER$_N$ and capacitance values of control cells were 1016 ± 124 ohms*cm^2 and $5.19*10^{-7} \pm 2.55*10^{-8}$ microfarads/cm^2, respectively. *C* and *D*, concentration-dependent Mn transfer to the respective acceptor (not incubated) compartment (*C*), percentage, normalized to the incubation concentration, Mn transfer (*D*) after apical or basolateral MnCl$_2$ incubation. *E*, Mn permeability coefficients and respective permeability coefficients of the permeability marker [^{14}C]sucrose after 72 h MnCl$_2$ apical or basolateral incubation. *F*, Mn permeability after concurrent MnCl$_2$ incubation of both compartments. *C–F*, mean values of least three independent determinations with three replicates $\pm$ S.D. (*error bars*); *a → b*, apical-to-basolateral transfer; *b → a*, basolateral-to-apical transfer.

NSC306711, Mn basolateral-to-apical transfer was not significantly different compared with the studies without the inhibitor (data not shown).

Effect of Ca on Manganese-induced Blood-CSF Barrier Disturbance—Further studies determining the impact of calcium (Ca) on Mn-induced disturbance of blood-CSF barrier properties refer to a reconstitution of barrier properties by Ca postincubation. Thus, filters of the *in vitro* blood-CSF barrier model were treated with 200 μM MnCl$_2$ at the basolateral compartment to strongly disturb barrier integrity and function. After 24 h of MnCl$_2$ incubation, the basolateral medium was replaced with SFM (containing approximately 1000 μM Ca) or CaCl$_2$-enriched medium (SFM + 250 or 500 μM Ca). In case of a postincubation with SFM or Ca-enriched SFM, a reconstitution of the barrier tightness was clearly visible as measured by an increase of the respective TEER$_P$ values (Fig. 5*A*). Moreover,

capacitance values, active fluid secretion to the apical compartment, and transport of phenol red to the basolateral compartment increased again (data not shown). Concordantly, the [^{14}C]sucrose studies revealed the restored barrier tightness after Ca postincubation (Fig. 5*B*). As expected, the replacement of the basolateral medium did not result in a reduction of the apical Mn concentration (data not shown).

The barrier properties of the epithelial cell monolayer were further investigated by the immunocytochemical analysis of occludin, a protein that is a central functional component of tight junctions (32). In nonexposed PCPECs, occludin staining appeared (33) in clear lines, without any fuzzy appearance, and cell borders were mostly straight and not serrated (Fig. 5*CI*). In contrast, filters treated for 24 h with 200 μM MnCl$_2$ (Fig. 5*CII*) showed more serrated and perforated cell borders, indicating that tight junctions were not fully closed anymore.
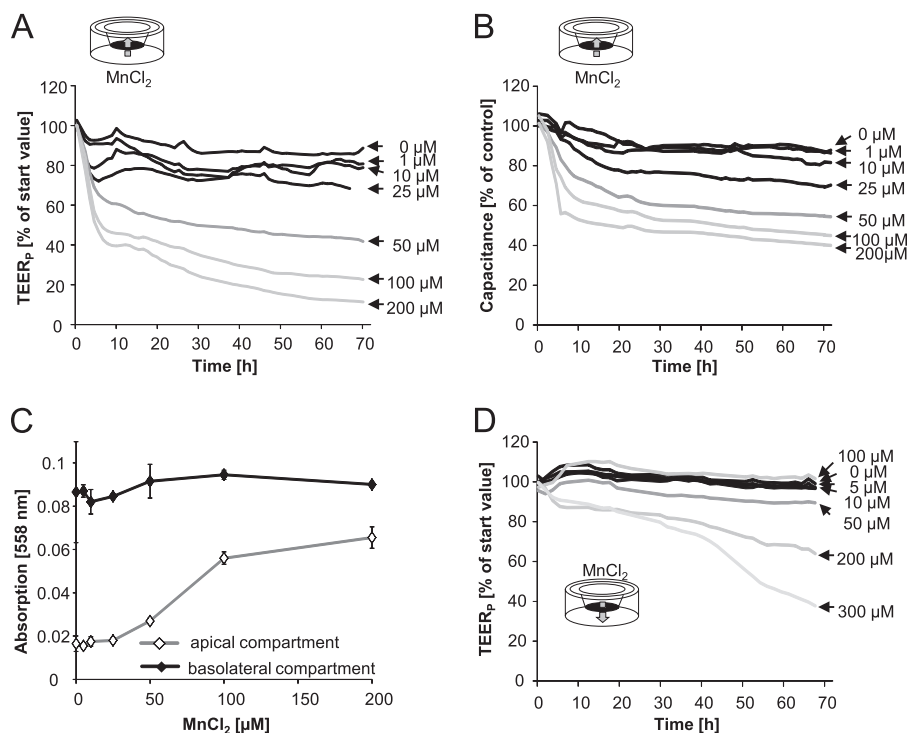
FIGURE 3. **Mn and *in vitro* blood-CSF barrier.** *A* and *B*, impact of $MnCl_2$ on the barrier integrity ($TEER_P$) (*A*) and the capacitance (*B*) after basolateral $MnCl_2$ incubation. Data, expressed as percentage of start value, represent mean values of at least three independent determinations with three replicates each with S.D. $< \pm 10\%$. Mean $TEER_P$ and capacitance values of control cells were 801 ± 96 ohms*cm^2 and $3.75*10^{-6} \pm 2.09*10^{-7}$ microfarads/cm^2, respectively. *C*, phenol red concentration measured at 558 nm after 72-h basolateral $MnCl_2$ incubation. Shown are mean values of least three independent determinations with three replicates $\pm$ S.D. (*error bars*). *D*, influence of $MnCl_2$ on the $TEER_P$ values after apical $MnCl_2$ incubation. Data, expressed as percentage of start value, represent mean values of at least three independent determinations with three replicates with S.D. $< \pm 10\%$.

Apparently, the subsequent replacement of the basolateral $MnCl_2$-incubated medium with Ca-enriched SFM resulted in a relock of the tight junctions, leaving only a few areas with not fully closed tight junctions (Fig. 5*CIII*). Comparable studies using the *in vitro* BBB model, in which 200 μM $MnCl_2$ were preincubated to the apical compartment for 24 h and then postincubated with SFM or Ca-enriched SFM, demonstrate no reversibility of the Mn- induced effects in this model (data not shown).

Manganese and Na^+,K^+-ATPase in Blood-CSF Barrier—The role of Na^+-K^+-ATPase in Mn transfer was studied via a basolateral incubation with its selective inhibitor ouabain immediately prior to apical or basolateral incubation with 10 μM $MnCl_2$. Within the following 72 h neither the basolateral-to-apical nor the apical-to-basolateral transfer was significantly different from the studies in the absence of ouabain (Fig. 6*A*). At the same time, Na^+-K^+-ATPase activity was clearly affected, as measured by an increase of the phenol red concentration on the apical side.

Immunological Na^+-K^+-ATPase staining reveals that in nonexposed as well as ouabain-treated (24–72 h) cells Na^+,K^+-ATPase is located at the luminal surface (Fig. 6*B*, *I* and *II*). In contrast, filters that were treated for 24 h with 200 μM $MnCl_2$ in the basolateral compartment had a significantly reduced Na^+,K^+-ATPase signal (Fig. 6*BIII*); a 72-h incubation with $MnCl_2$ showed similar effects (data not shown). After an additional 48 h postincubation with $CaCl_2$, Na^+,K^+-ATPase is located again at the luminal surface (Fig. 6*BIV*).

DISCUSSION

A crucial poorly understood step in Mn-induced neurotoxicity is its effect on and its transfer across the two brain-regulating interfaces, the BBB and the blood-CSF barrier. In the present study, well established porcine-based cell culture models were used, with PBCECs and PCPECs as structural basis of the BBB and the blood-CSF barrier, respectively. It is well known that pig brain shows more similarities to human brain, with respect to size, anatomy growth, and development compared with brains of other laboratory animals including rodents. This makes porcine *in vitro* systems important experimental models to be considered within neurosciences (34–36). Additionally, these primary cultures obtained from freshly slaughtered pigs have the clear advantage of being an alternative approach to the costly, time-consuming and ethically questionable systems derived from experimental animals.

Regarding the *in vitro* BBB studies in the present work, the data clearly show that barrier leakage caused by $\geq$200 μM $MnCl_2$ in the apical, blood-resembling compartment correlated with Mn cytotoxicity. Results obtained from $TEER_N$ measurements were confirmed by [^{14}C]sucrose permeability studies, which similarly indicated an alteration of paracellular tightness in the presence of elevated Mn concentrations. In contrast, a basolateral $MnCl_2$ incubation, which simulates an *in vivo* situation after Mn accumulation in specific brain regions (37), did not affect barrier integrity up to 500 μM $MnCl_2$, a concentration clearly being not exposure-relevant anymore. In brain tissues, physiological Mn concentrations range from 2 to
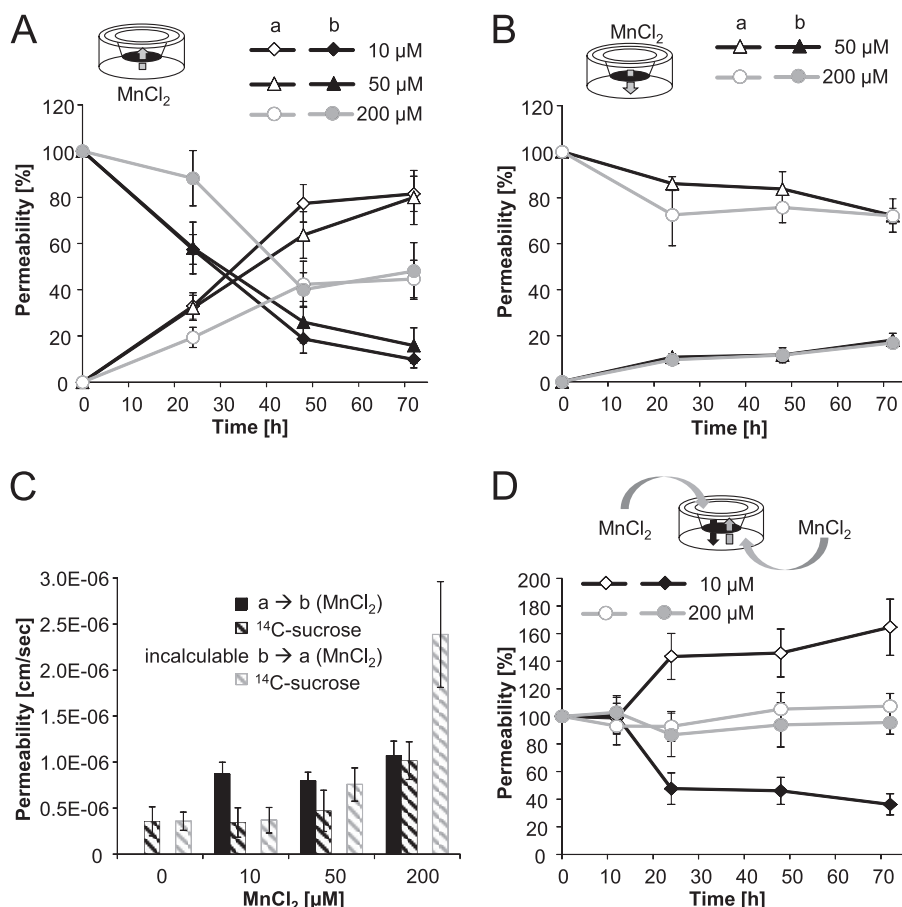
FIGURE 4. **Mn transfer across the *in vitro* blood-CSF barrier.** *A* and *B*, Mn transfer after MnCl₂ incubation of the basolateral compartment (influx studies) (*A*) or the apical compartment (efflux studies) (*B*). Data are expressed as percentage of the respective incubated MnCl₂ concentration; *open symbols* represent quantified Mn concentrations in the apical, *filled symbols* in the basolateral compartment. *C*, Mn permeability coefficients and respective permeability coefficients of the permeability marker [¹⁴C]sucrose after 72-h MnCl₂ basolateral or apical incubation. Due to missing linearity basolateral-to-apical, Mn permeability coefficient cannot be calculated. *D*, Mn permeability after concurrent MnCl₂ incubation of both compartments. *A–D*, data represent mean values of at least three independent determinations with three replicates each ± S.D. (*error bars*). *a*, apical compartment; *b*, basolateral compartment; *a → b*, apical-to-basolateral transfer; *b → a*, basolateral-to-apical transfer.

8 μM, but can be increased severalfold upon overexposure (38, 39). Together with the observed small Mn efflux in case of high Mn concentrations ($\geq$100 μM) to the apical compartment (blood side), these results are in agreement with *in vivo* studies, in which Mn after entering the brain, strongly persists, and therefore accumulates in the brain (40, 41). Evidence suggests that brain Mn efflux across the BBB proceeds through slow diffusion (42), which is supported by our data. In the case of lower applied MnCl₂ concentrations ($\leq$50 μM), comparable apical-to-basolateral (influx) and basolateral-to-apical (efflux) transfer rates after incubation in one of the respective compartments as well as the missing Mn accumulation in one compartment after parallel incubation on both, apical and basolateral, sides, strongly point to a passive transfer process of Mn across the BBB. The influx permeability coefficient across the BBB for divalent Mn is, for example, comparable with the influx permeability coefficient of morphine in the same *in vitro* model (25).

One very important outcome of the present work is the fact that in direct comparison with the *in vitro* BBB model, the blood-CSF barrier model was much more sensitive toward Mn. The disturbance of barrier properties was not caused by Mn cytoxicity. The observed higher cytotoxic resistance and Mn bioavailability in PCPECs compared with PBCECs suit with *in*

vivo studies, demonstrating a several orders of magnitude higher Mn uptake and accumulation by the CP in comparison with other brain regions (43).

Similar to the BBB model, blood-CSF barrier properties were most strongly affected after MnCl₂ incubation on the blood side, which is in the blood-CSF barrier model the basolateral compartment. Thus, barrier tightness and functions were strongly disturbed after basolateral incubation with $\geq$50 μM MnCl₂ and apical incubation with $\geq$200 μM MnCl₂, respectively. Moreover, apical-to-basolateral Mn transfer was much lower compared with basolateral-to-apical transfer, which has very recently also been reported in a rat-based blood-CSF barrier model (44).

The observed Mn-induced decrease of active fluid secretion and phenol red transport might be due to an inhibition of Na$^+$,K$^+$-ATPase function by Mn. In the CP epithelium, the Na$^+$,K$^+$-ATPase is the driving force of the active fluid secretion and is furthermore a major player of various active transport properties including transport of phenol red from apical to basolateral compartment. Disturbance of Na$^+$,K$^+$-ATPase function might result from an inhibition of the Na$^+$,K$^+$-ATPase activity, which has been described in neuroblastoma cells or liver tissue by Mn before (45, 46), but might also be due
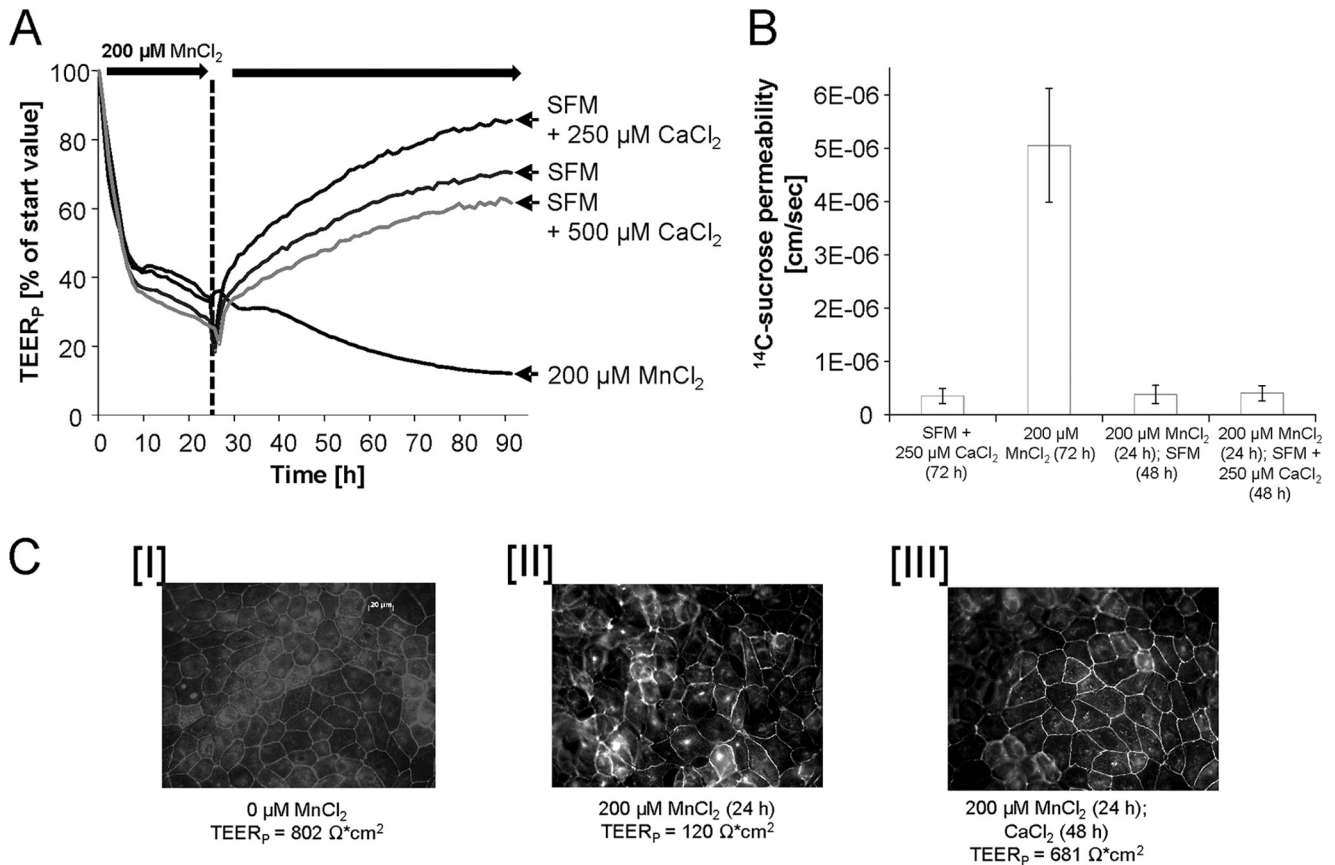
FIGURE 5. **Effect of Ca on the Mn-induced blood-CSF barrier disturbance.** *A* and *B*, relative $TEER_P$ values (*A*) and respective [^{14}C]sucrose permeability coefficients (*B*) after 24-h preincubation with 200 μM $MnCl_2$, medium exchange at the basolateral compartment and postincubation without/with Ca-enriched medium (Ca concentration in medium of the CP epithelial cells: 1013 μM). Shown are data from one representative experiment (*n* = 3 with S.D. < ±10% (*error bars*)). *C*, immunocytochemical staining of occludin. *I*, nontreated ($TEER_P$ = 802 ohms*cm^2) barriers; *II*, barriers after basolateral incubation with 200 μM $MnCl_2$ for 24 h ($TEER_P$ = 120 ohms*cm^2); and *III*, barriers after 24-h basolateral preincubation with $MnCl_2$ and 48 h after incubation with Ca-enriched SFM (SFM + 250 μM $CaCl_2$ ($TEER_P$ = 681 ohms*cm^2).
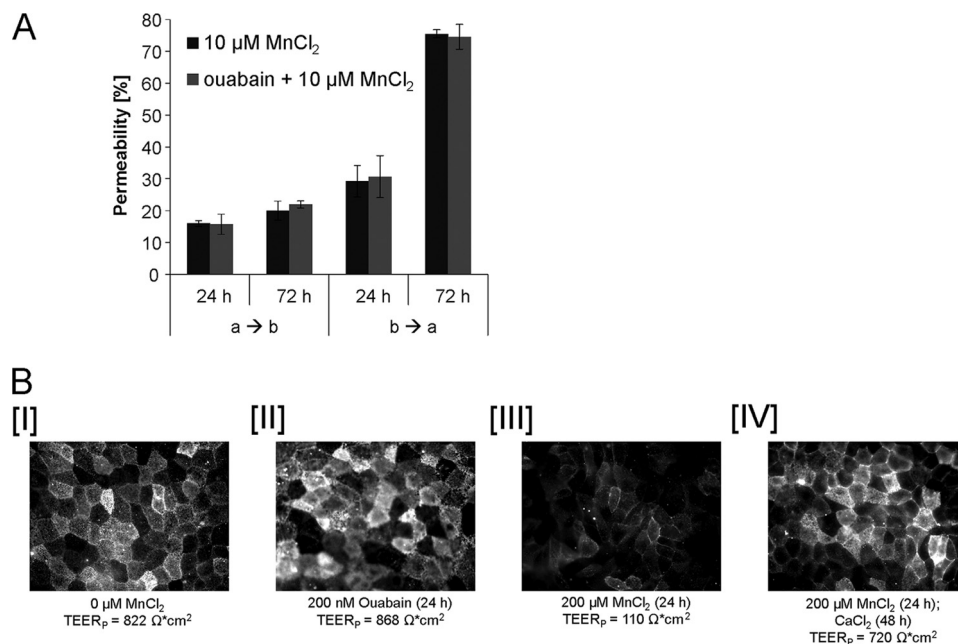

FIGURE 6. **Mn transfer across the *in vitro* blood-CSF barrier without/with the Na$^+$,K$^+$-ATPase-inhibitor ouabain (200 nM).** *A*, mean values of three determinations ± S.D. (*error bars*). *B*, immunocytochemical staining of the Na$^+$,K$^+$-ATPase. *I*, nontreated ($TEER_P$ = 822 ohms*cm^2) barriers; *II*, barriers after basolateral incubation with 200 nM ouabain for 72 h ($TEER_P$ = 868 ohms*cm^2); *III*, barriers after basolateral incubation with 200 μM $MnCl_2$ for 24 h ($TEER_P$ = 110 ohms*cm^2); and *IV*, barriers after 24-h basolateral preincubation with $MnCl_2$ and 48 h after incubation with Ca-enriched SFM (SFM + 250 μM $CaCl_2$ ($TEER_P$ = 720 ohms*cm^2). *a → b*, apical-to-basolateral transfer; *b → a*, basolateral-to-apical transfer.

to Na^+,K^+-ATPase internalization following a phosphorylation of a Na^+,K^+-ATPase subunit. The immunocytochemistry studies carried out in this work strongly argue for such a Na^+,K^+-ATPase internalization in the presence of high $MnCl_2$ concentrations. Na^+,K^+-ATPase has also been reported to be inhibited by ROS in primary cultures (47), and it is generally known that Mn overexposure induces a transient increase in the cellular ROS level of brain cells (48, 49). Additionally, chronic Mn exposure might alter systematic homeostasis of calcium, leading to a further impairment of Na^+,K^+-ATPase function (14, 50). As a further barrier integrity disturbing mechanism, occludin immunocytochemistry studies reveal a disturbance of tight junction structure, which might also be partly caused by an inhibition of Na^+,K^+-ATPase function (51).

Regarding the type of Mn influx via the blood-CSF barrier, our data argue for an active transport mechanism. As summarized in Ref. 44, many transporters are expressed in the CP and are therefore discussed to contribute to Mn transport. Because DMT1 has been shown to be present in the blood-CSF barrier in several studies and Mn exposure resulted in an increased DMT1 expression in rats (52), the present study intended to assess the role of DMT1 in Mn transfer processes. However, applying the DMT1 inhibitor NSC306711, our data show that in the applied *in vitro* system DMT1 is not the major transporter for Mn uptake into the brain via the blood-CSF barrier. These data account with studies in which Mn uptake was not significantly reduced in homozygous Belgrade rat (b/b) with no functional DMT1 expression (53). The application of the selective Na^+,K^+-ATPase inhibitor ouabain did not result in an decrease of Mn transfer across the blood-CSF barrier, indicating that Mn transfer is independent of Na^+,K^+-ATPase function, which has been published by Crossgrove and Yokel before (54). In contrast, recent evidence has clearly shown that in a rat model upon Mn treatment, MTP1 (also named ferroportin 1) is visibly translocated from the diffuse distribution in the cytosol to apical microvilli of the CP and transports excess amounts of intracellular Mn toward the CSF. Furthermore, it is interesting to note that similar to MTP1, the direction of cellular TfR trafficking was also toward the CSF (55).

Mn uptake in the CP has been reported to be stronger than in other brain regions, whereas Mn concentrations in CSF are comparably low, indicating no strong Mn efflux from CP into CSF. Thus, physiological Mn concentrations in CSF are comparable with serum concentrations, ranging from 1.0 ± 0.5 μg/liter in nonexposed patients to severalfold higher levels in exposed patients (56, 57). This fact might have contributed to the assumption frequently discussed in literature that Mn enters the brain at normal physiological plasma concentrations across the capillary endothelium, whereas at high plasma concentrations, Mn transfer across the CP appears to predominate (3, 43). However, taking into account the data in this work, in which for the first time Mn transfer across the two barriers has been compared in one study, this assumption has to be critically assessed.

Moreover, in the present study we showed for the first time that a basolateral postincubation with Ca can compensate for Mn-induced disturbance of blood-CSF barrier properties, restoring both barrier tightness and function. Intracellular Ca homeostasis has a strong impact on tight junction integrity, and a decrease in intracellular Ca levels has been shown to alter subcellular localization of occludin and changes Zo-1/actin binding (58). In biological systems, Mn^{2+} has the same charge and relative size as Ca^{2+}, and a number of reports have shown that Mn and Ca trafficking, recruitment, and storage are regulated by the same ion pumps and intracellular compartments. Therefore, Mn^{2+} might compete with Ca^{2+} in uptake studies (59, 60), thereby disturb intracellular Ca homeostasis and correct tight junction formation and/or localization (26, 61). This effect might be reversible by elevated Ca concentrations, as indicated by the present occludin immunofluorescence studies. Moreover, a recovery of Na^+,K^+-ATPase function, which is also coupled to intracellular Ca homeostasis, might also contribute to the observed Ca-mediated reversibility of Mn-induced barrier disturbance. Further studies should examine these interactions in more detail, which might also help to understand the mechanism of Mn-induced barrier disruption.

CONCLUSION

By the use of state-of-the *in vitro* barrier models effects of Mn on the integrity of the blood-brain and blood-CSF barrier as well as Mn transfer across these two barriers in both directions were compared in one study for the first time. In summary, both the observed stronger Mn sensitivity of the *in vitro* blood-CSF barrier and the observed site-directed, most probably active Mn transport toward the brain facing compartment, reveal that, in contrast to the general assumption in literature, the blood-CSF barrier might be the major route for Mn into the brain after oral Mn intake.

REFERENCES

1. Santamaria, A. B. (2008) Manganese exposure, essentiality and toxicity. *Indian J. Med. Res.* **128,** 484–500
2. Olanow, C. W. (2004) Manganese-induced parkinsonism and Parkinson's disease. *Ann. N.Y. Acad. Sci.* **1012,** 209–223
3. Aschner, M., Guilarte, T. R., Schneider, J. S., and Zheng, W. (2007) Manganese: recent advances in understanding its transport and neurotoxicity. *Toxicol. Appl. Pharmacol.* **221,** 131–147
4. Bowler, R. M., Gysens, S., Diamond, E., Nakagawa, S., Drezgic, M., and Roels, H. A. (2006) Manganese exposure: neuropsychological and neurological symptoms and effects in welders. *Neurotoxicology* **27,** 315–326
5. Guilarte, T. R. (2010) Manganese and Parkinson's disease: a critical review and new findings. *Environ. Health Perspect.* **118,** 1071–1080
6. Pan, D., Caruthers, S.D., Senpan, A., Schmieder, A. H., Wickline, S., and Lanza, G. M. (2010) Revisiting an old friend: manganese-based MRI contrast agents. *Wiley Interdiscip. Rev. Nanomed. Nanobiotechnol.* 10.1002/wnan.116
7. Nagatomo, S., Umehara, F., Hanada, K., Nobuhara, Y., Takenaga, S., Arimura, K., and Osame, M. (1999) Manganese intoxication during total parenteral nutrition: report of two cases and review of the literature. *J. Neurol. Sci.* **162,** 102–105
8. Gerber, G. B., Léonard, A., and Hantson, P. (2002) Carcinogenicity, mutagenicity and teratogenicity of manganese compounds. *Crit. Rev. Oncol.*

Hematol. **42,** 25–34

9. Flynn, M. R., and Susi, P. (2009) Neurological risks associated with manganese exposure from welding operations: a literature review. *Int. J. Hyg. Environ. Health* **212,** 459–469

10. Abbott, N. J., Patabendige, A. A., Dolman, D. E., Yusof, S. R., and Begley, D. J. (2010) Structure and function of the blood-brain barrier. *Neurobiol. Dis.* **37,** 13–25

11. Strazielle, N., and Ghersi-Egea, J. F. (2000) Choroid plexus in the central nervous system: biology and physiopathology. *J. Neuropathol. Exp. Neurol.* **59,** 561–574

12. Rabin, O., Hegedus, L., Bourre, J. M., and Smith, Q. R. (1993) Rapid brain uptake of manganese(II) across the blood-brain barrier. *J. Neurochem.* **61,** 509–517

13. Fitsanakis, V. A., Piccola, G., Marreilha dos Santos, A. P., Aschner, J. L., and Aschner, M. (2007) Putative proteins involved in manganese transport across the blood-brain barrier 1ier. *Hum. Exp. Toxicol.* **26,** 295–302

14. Bowman, A. B., Kwakye, G. F., Hernández, E. H., and Aschner, M. (2011) Role of manganese in neurodegenerative diseases. *J. Trace Elem. Med. Biol.* **25,** 191–203

15. Nagasawa, K., Escartin, C., and Swanson, R. A. (2009) Astrocyte cultures exhibit P2X7 receptor channel opening in the absence of exogenous ligands. *Glia* **57,** 622–633

16. Yokel, R. A. (2006) Blood-brain barrier flux of aluminum, manganese, iron and other metals suspected to contribute to metal-induced neurodegeneration. *J. Alzheimers Dis.* **10,** 223–253

17. Aschner, M., and Gannon, M. (1994) Manganese (Mn) transport across the rat blood-brain barrier: saturable and transferrin-dependent transport mechanisms. *Brain Res. Bull.* **33,** 345–349

18. Crossgrove, J. S., Allen, D. D., Bukaveckas, B. L., Rhineheimer, S. S., and Yokel, R. A. (2003) Manganese distribution across the blood-brain barrier. I. Evidence for carrier-mediated influx of manganese citrate as well as manganese and manganese transferrin. *Neurotoxicology* **24,** 3–13

19. von Wedel-Parlow, M., Wölte, P., and Galla, H. J. (2009) Regulation of major efflux transporters under inflammatory conditions at the blood-brain barrier *in vitro*. *J. Neurochem.* **111,** 111–118

20. Angelow, S., Zeni, P., and Galla, H. J. (2004) Usefulness and limitation of primary cultured porcine choroid plexus epithelial cells as an *in vitro* model to study drug transport at the blood-CSF barrier. *Adv. Drug Deliv. Rev.* **56,** 1859–1873

21. Gath, U., Hakvoort, A., Wegener, J., Decker, S., and Galla, H. J. (1997) Porcine choroid plexus cells in culture: expression of polarized phenotype, maintenance of barrier properties and apical secretion of CSF-components. *Eur. J. Cell Biol.* **74,** 68–78

22. Franke, H., Galla, H. J., and Beuckmann, C. T. (1999) An improved low-permeability *in vitro* model of the blood-brain barrier: transport studies on retinoids, sucrose, haloperidol, caffeine and mannitol. *Brain Res.* **818,** 65–71

23. Kröll, S., El-Gindi, J., Thanabalasundaram, G., Panpumthong, P., Schrot, S., Hartmann, C., and Galla, H. J. (2009) Control of the blood-brain barrier by glucocorticoids and the cells of the neurovascular unit. *Ann. N.Y. Acad. Sci.* **1165,** 228–239

24. Haselbach, M., Wegener, J., Decker, S., Engelbertz, C., and Galla, H. J. (2001) Porcine choroid plexus epithelial cells in culture: regulation of barrier properties and transport processes. *Microsc. Res. Tech.* **52,** 137–152

25. Lohmann, C., Hüwel, S., and Galla, H. J. (2002) Predicting blood-brain barrier permeability of drugs: evaluation of different *in vitro* assays. *J. Drug Target* **10,** 263–276

26. Lischper, M., Beuck, S., Thanabalasundaram, G., Pieper, C., and Galla, H. J. (2010) Metalloproteinase-mediated occludin cleavage in the cerebral microcapillary endothelium under pathological conditions. *Brain Res.* **1326,** 114–127

27. Hakvoort, A., Haselbach, M., Wegener, J., Hoheisel, D., and Galla, H. J. (1998) The polarity of choroid plexus epithelial cells *in vitro* is improved in serum-free medium. *J. Neurochem.* **71,** 1141–1150

28. Repetto, G., del Peso, A., and Zurita, J. L. (2008) Neutral red uptake assay for the estimation of cell viability/cytotoxicity. *Nat. Protoc.* **3,** 1125–1131

29. Wehe, C. A., Bornhorst, J., Holtkamp, M., Sperling, M., Galla, H. J., Schwerdtle, T., and Karst, U. (2011) Fast and low sample consuming quantifi-cation of manganese in cell nutrient solutions by flow injection ICP-QMS. *Metallomics* **3,** 1291–1296

30. Michalke, B., Halbach, S., and Nischwitz, V. (2007) Speciation and toxicological relevance of manganese in humans. *J. Environ. Monit.* **9,** 650–656

31. Buckett, P. D., and Wessling-Resnick, M. (2009) Small molecule inhibitors of divalent metal transporter-1. *Am. J. Physiol. Gastrointest. Liver Physiol.* **296,** G798–804

32. McCarthy, K. M., Skare, I. B., Stankewich, M. C., Furuse, M., Tsukita, S., Rogers, R. A., Lynch, R. D., and Schneeberger, E. E. (1996) Occludin is a functional component of the tight junction. *J. Cell Sci.* **109,** 2287–2298

33. Franke, H., Galla, H., and Beuckmann, C. T. (2000) Primary cultures of brain microvessel endothelial cells: a valid and flexible model to study drug transport through the blood-brain barrier *in vitro*. *Brain Res. Brain Res. Protoc.* **5,** 248–256

34. Swanson, L. W. (1995) Mapping the human brain: past, present, and future. *Trends Neurosci.* **18,** 471–474

35. Lind, N. M., Moustgaard, A., Jelsing, J., Vajta, G., Cumming, P., and Hansen, A. K. (2007) The use of pigs in neuroscience: modeling brain disorders. *Neurosci. Biobehav. Rev.* **31,** 728–751

36. Podolska, A., Kaczkowski, B., Kamp Busk, P., Søkilde, R., Litman, T., Fredholm, M., and Cirera, S. (2011) MicroRNA expression profiling of the porcine developing brain. *PLoS One* **6,** e14494

37. Santamaria, A. B., and Sulsky, S. I. (2010) Risk assessment of an essential element: manganese. *J. Toxicol. Environ. Health A* **73,** 128–155

38. Pal, P. K., Samii, A., and Calne, D. B. (1999) Manganese neurotoxicity: a review of clinical features, imaging and pathology. *Neurotoxicology* **20,** 227–238

39. Liu, X., Sullivan, K. A., Madl, J. E., Legare, M., and Tjalkens, R. B. (2006) Manganese-induced neurotoxicity: the role of astroglial-derived nitric oxide in striatal interneuron degeneration. *Toxicol. Sci.* **91,** 521–531

40. Dastur, D. K., Manghani, D. K., and Raghavendran, K. V. (1971) Distribution and fate of ^{54}Mn in the monkey: studies of different parts of the central nervous system and other organs. *J. Clin. Invest.* **50,** 9–20

41. Takeda, A., Sawashita, J., and Okada, S. (1995) Biological half-lives of zinc and manganese in rat brain. *Brain Res.* **695,** 53–58

42. Yokel, R. A., Crossgrove, J. S., and Bukaveckas, B. L. (2003) Manganese distribution across the blood-brain barrier. II. Manganese efflux from the brain does not appear to be carrier mediated. *Neurotoxicology* **24,** 15–22

43. Murphy, V. A., Wadhwani, K. C., Smith, Q. R., and Rapoport, S. I. (1991) Saturable transport of manganese(II) across the rat blood-brain barrier. *J. Neurochem.* **57,** 948–954

44. Schmitt, C., Strazielle, N., Richaud, P., Bouron, A., and Ghersi-Egea, J. F. (2011) Active transport at the blood-CSF barrier contributes to manganese influx into the brain. *J. Neurochem.* **117,** 747–756

45. Chtourou, Y., Trabelsi, K., Fetoui, H., Mkannez, G., Kallel, H., and Zeghal, N. (2011) Manganese induces oxidative stress, redox state unbalance and disrupts membrane bound ATPases on murine neuroblastoma cells *in vitro*: protective role of silymarin. *Neurochem. Res.* **36,** 1546–1557

46. Huang, P., Li, G., Chen, C., Wang, H., Han, Y., Zhang, S., Xiao, Y., Zhang, M., Liu, N., Chu, J., Zhang, L., and Sun, Z. (2012) Differential toxicity of Mn^{2+} and Mn^{3+} to rat liver tissues: oxidative damage, membrane fluidity and histopathological changes. *Exp. Toxicol. Pathol.* **64,** 197–203

47. Rodrigo, R., Bächler, J. P., Araya, J., Prat, H., and Passalacqua, W. (2007) Relationship between (Na + K)-ATPase activity, lipid peroxidation and fatty acid profile in erythrocytes of hypertensive and normotensive subjects. *Mol. Cell Biochem.* **303,** 73–81

48. Milatovic, D., Zaja-Milatovic, S., Gupta, R. C., Yu, Y., and Aschner, M. (2009) Oxidative damage and neurodegeneration in manganese-induced neurotoxicity. *Toxicol. Appl. Pharmacol.* **240,** 219–225

49. Marreilha Dos Santos, A. P., Lopes Santos, M., Batoréu, M. C., and Aschner, M. (2011) Prolactin is a peripheral marker of manganese neurotoxicity. *Brain Res.* **1382,** 282–290

50. Therien, A. G., and Blostein, R. (2000) Mechanisms of sodium pump regulation. *Am. J. Physiol. Cell Physiol.* **279,** C541–566

51. Rajasekaran, S. A., Hu, J., Gopal, J., Gallemore, R., Ryazantsev, S., Bok, D., and Rajasekaran, A. K. (2003) Na,K-ATPase inhibition alters tight junction structure and permeability in human retinal pigment epithelial cells. *Am. J. Physiol. Cell Physiol.* **284,** C1497–1507

52. Wang, X., Li, G. J., and Zheng, W. (2006) Up-regulation of DMT1 expression in choroidal epithelia of the blood-CSF barrier following manganese exposure *in vitro*. *Brain Res*. **1097,** 1–10

53. Crossgrove, J., and Zheng, W. (2004) Manganese toxicity upon overexposure. *NMR Biomed* **17,** 544–553

54. Crossgrove, J. S., and Yokel, R. A. (2005) Manganese distribution across the blood-brain barrier. IV. Evidence for brain influx through store-operated calcium channels. *Neurotoxicology* **26,** 297–307

55. Wang, X., Miller, D. S., and Zheng, W. (2008) Intracellular localization and subsequent redistribution of metal transporters in a rat choroid plexus model following exposure to manganese or iron. *Toxicol. Appl. Pharmacol*. **230,** 167–174

56. Nischwitz, V., Berthele, A., and Michalke, B. (2008) Speciation analysis of selected metals and determination of their total contents in paired serum and cerebrospinal fluid samples: an approach to investigate the permeability of the human blood-cerebrospinal fluid barrier. *Anal. Chim. Acta*

627, 258–269

57. Hozumi, I., Hasegawa, T., Honda, A., Ozawa, K., Hayashi, Y., Hashimoto, K., Yamada, M., Koumura, A., Sakurai, T., Kimura, A., Tanaka, Y., Satoh, M., and Inuzuka, T. (2011) Patterns of levels of biological metals in CSF differ among neurodegenerative diseases. *J. Neurol. Sci*. **303,** 95–99

58. Ye, J., Tsukamoto, T., Sun, A., and Nigam, S. K. (1999) A role for intracellular calcium in tight junction reassembly after ATP depletion-repletion. *Am. J. Physiol*. **277,** F524–532

59. Ambudkar, I. S., Lockwich, T., Hiramatsu, Y., and Baum, B. J. (1992) Calcium entry in rat parotid acinar cells. *Mol. Cell. Biochem*. **114,** 73–77

60. Yokel, R. A. (2009) Manganese flux across the blood-brain barrier. *Neuromolecular Med*. **11,** 297–310

61. Wong, V. (1997) Phosphorylation of occludin correlates with occludin localization and function at the tight junction. *Am. J. Physiol*. **273,** C1859–1867